11-5-2018

Human-like hyperplastic prostate with low ZIP1 induced solely by Zn deficiency in rats.

Louise Y. Fong
Thomas Jefferson University

Ruiyan Jing
Thomas Jefferson University

Karl J. Smalley
Thomas Jefferson University

Zi-Xuan Wang
Thomas Jefferson University

Cristian Taccioli
University of Padova

See next page for additional authors

Recommended Citation

Fong, Louise Y.; Jing, Ruiyan; Smalley, Karl J.; Wang, Zi-Xuan; Taccioli, Cristian; Fan, Sili; Chen, Hongping; Alder, Hansjuerg; Huebner, Kay; Farber, John L.; Fiehn, Oliver; and Croce, Carlo M., "Human-like hyperplastic prostate with low ZIP1 induced solely by Zn deficiency in rats." (2018). *Department of Pathology, Anatomy, and Cell Biology Faculty Papers.* Paper 257.
https://jdc.jefferson.edu/pacbfp/257

Human-like hyperplastic prostate with low ZIP1 induced solely by Zn deficiency in rats

Louise Y. Fong[a,b,1], Ruiyan Jing[a], Karl J. Smalley[b], Zi-Xuan Wang[a], Cristian Taccioli[c], Sili Fan[d], Hongping Chen[b,2], Hansjuerg Alder[e,f], Kay Huebner[e,f], John L. Farber[a], Oliver Fiehn[d,g], and Carlo M. Croce[e,f,1]

[a]Department of Pathology, Anatomy, and Cell Biology, Thomas Jefferson University, Philadelphia, PA 19107; [b]Sidney Kimmel Cancer Center, Thomas Jefferson University, Philadelphia, PA 19107; [c]Department of Animal Medicine, Health and Production, University of Padova, 35122 Padova PD, Italy; [d]National Institutes of Health West Coast Metabolomics Center, University of California Davis Genome Center, University of California, Davis, CA 95616; [e]Department of Cancer Biology and Genetics, The Ohio State University, Columbus, OH 43210; [f]The Comprehensive Cancer Center, The Ohio State University, Columbus, OH 43210; and [g]Department of Biochemistry, Faculty of Sciences, King Abdulaziz University, 21589 Jeddah, Saudi Arabia

Contributed by Carlo M. Croce, October 15, 2018 (sent for review August 15, 2018; reviewed by Cory Abate-Shen and Dan Theodorescu)

Prostate cancer is a leading cause of cancer death in men over 50 years of age, and there is a characteristic marked decrease in Zn content in the malignant prostate cells. The cause and consequences of this loss have thus far been unknown. We found that in middle-aged rats a Zn-deficient diet reduces prostatic Zn levels ($P = 0.025$), increases cellular proliferation, and induces an inflammatory phenotype with COX-2 overexpression. This hyperplastic/inflammatory prostate has a human prostate cancer-like microRNA profile, with up-regulation of the Zn-homeostasis–regulating miR-183-96-182 cluster (fold change = 1.41–2.38; $P = 0.029$–0.0003) and down-regulation of the Zn importer ZIP1 (target of miR-182), leading to a reduction of prostatic Zn. This inverse relationship between miR-182 and ZIP1 also occurs in human prostate cancer tissue, which is known for Zn loss. The discovery that the Zn-depleted middle-aged rat prostate has a metabolic phenotype resembling that of human prostate cancer, with a 10-fold down-regulation of citric acid ($P = 0.0003$), links citrate reduction directly to prostatic Zn loss, providing the underlying mechanism linking dietary Zn deficiency with miR-183-96-182 overexpression, ZIP1 down-regulation, prostatic Zn loss, and the resultant citrate down-regulation, changes mimicking features of human prostate cancer. Thus, dietary Zn deficiency during rat middle age produces changes that mimic those of human prostate carcinoma and may increase the risk for prostate cancer, supporting the need for assessment of Zn supplementation in its prevention.

dietary Zn intake | prostate cancer risk | untargeted miRNA profiling | untargeted metabolomics profiling | prostate cancer metabolic phenotype

Prostate cancer (PCa) is a leading cause of cancer death in men over the age of 50 y. It has a long induction period, as many men in their 30s have incipient prostate lesions (1). Risk factors include age, race/ethnicity, family history, and diet, with age being the most consistent factor (2).

Zn is important for maintaining prostate health. Zn levels are ∼15-fold higher in normal human prostate gland than in other tissues (3) but are reduced ∼60–80% in PCa tissue (3–5). The decrease in prostatic Zn concentration occurs early in PCa development (6). This inability to accumulate Zn in PCa tissues is due in part to the down-regulation of the Zn uptake transporters, notably hZIP1 (7–9) and hZIP2 and hZIP3 (10).

Dietary Zn deficiency is a significant health issue affecting ∼31% of the global population, with higher rates in developing countries (11). Severe Zn deficiency is uncommon, but mild-to-moderate Zn deficiency is prevalent throughout the world due to limited access to Zn-rich foods (oyster, shellfish, animal products) and the concentration of Zn-absorption inhibitors, such as phytates, in plant-based diets (11, 12). The elderly male population is particularly at risk for Zn deficiency, owing to physiological, social, and economic factors (13). Because Zn is required for the activity of >300 enzymes and the conformation of >2,000 transcription factors that control signaling pathways (14), Zn deficiency can predispose to disease by adversely affecting these processes. Zn deficiency is implicated in the pathogenesis of several human cancers, including PCa (15) and esophageal squamous cell carcinoma (16). The mechanisms involved in the influence of Zn deficiency on PCa risk are not known.

Laboratory studies have shown that Zn has antitumor effects against PCa (5). In vivo Zn has protective effects against spontaneous PCa development in TRAMP (transgenic adenocarcinoma of the mouse prostate) mice (17) and against carcinogen-induced prostate cancer initiation in Sprague–Dawley rats (18). By contrast, epidemiologic studies regarding the effects of dietary Zn on PCa have produced inconsistent results (19–23). A 2003 study (19) reported that supplemental Zn at doses up to 100 mg/d was not associated with PCa risk but that long-term intake of doses >100 mg/d increased the risk of advanced PCa. More recent reports in 2009 and 2011 (21, 22) and an earlier 1999 study (20) showed that dietary/supplemental Zn protects against the development and progression of advanced PCa. Additionally, a 2016 case-control study found low dietary intake of Zn among African American patients with PCa, although the

Significance

Prostate cancer in man is associated with Zn loss, citrate metabolite reduction, overexpression of the miR-183-96-182 cluster, and regulation of Zn homeostasis through Zn transporter suppression. Our mechanistic study shows that a low-Zn diet upregulates this miR cluster in Zn-deficient middle-aged rat prostate, with ZIP1 mRNA/protein downregulation and a citrate-oxidizing metabolic phenotype, linking citrate reduction directly to prostatic Zn loss. The findings of this study show that the transcriptional and metabolic signal pathways induced by Zn deficiency in rats and almost certainly in men are critical for the development of human and rat prostate cancer and provide a strong rationale for including Zn supplementation in clinical trials to reduce the prostate cancer burden in the human population.

Author contributions: L.Y.F., K.H., J.L.F., and C.M.C. designed research; L.Y.F., R.J., Z.-X.W., S.F., H.C., H.A., and O.F. performed research; L.Y.F., K.J.S., C.T., K.H., J.L.F., O.F., and C.M.C. analyzed data; and L.Y.F., K.H., J.L.F., and C.M.C. wrote the paper.

Reviewers: C.A.-S., Columbia University Medical Center; and D.T., The Samuel Oschin Comprehensive Cancer Institute at Cedar-Sinai.

The authors declare no conflict of interest.

[1]To whom correspondence may be addressed. Email: louise.fong@jefferson.edu or carlo.croce@osumc.edu.

[2]Present address: Department of Histology and Embryology, Nanchang University, 33006 Nanchang, China.

This article contains supporting information online at www.pnas.org/lookup/suppl/doi:10.1073/pnas.1813956115/-/DCSupplemental.

findings were statistically nonsignificant; results of a meta-analysis did not support an association between Zn intake and PCa (23). Because epidemiological assessment of dietary Zn and Zn status during critical phases of human PCa carcinogenesis is challenging, animal models are needed to establish the association between dietary Zn intake and PCa risk.

Previously (24) we reported that in adult rats 23 wk of dietary Zn deficiency reduced tissue Zn level and altered miRNA expression in eight rat tissues, including prostate. miRNAs are noncoding RNAs that regulate gene expression by translational inhibition and mRNA degradation. miRNA expression levels are altered in all human cancers studied (25), including PCa (9, 26, 27). Additionally, miRNAs have emerged as key regulators of cellular metabolism in normal and pathological conditions (28).

Finally, normal human prostate cells exhibit a unique metabolic profile, with Zn accumulation and production of citrate in the tricarboxylic acid (TCA) cycle. PCa cells that lose the ability to accumulate Zn actively oxidize citrate, leading to a metabolic phenotype of reduced citrate levels (29, 30), as revealed by metabolomics studies (31, 32). Whether dietary Zn deficiency contributes to altered prostatic cellular metabolism has not been examined previously.

In this study, we recreated prostatic Zn loss in a middle-aged rat model and investigated whether with prostatic Zn loss, Zn deficiency also causes molecular alterations that may promote PCa initiation. We examined the consequences of prostatic Zn loss by analyzing Zn transporters, miRNA, and metabolomics profiles.

Results

A Zn-Deficient Middle-Aged Rat Prostate Model with Prostatic Zn Loss. This study was conducted in rat lateral prostate (hereafter called "prostate") that is embryologically homologous to the peripheral zone of human prostate where most PCa arises (33). Two rat strains were used: the traditional Sprague–Dawley strain and the Wistar-Unilever strain that is well characterized for prostate carcinogenesis research (34).

We sought to establish a Zn-depleted prostate model in middle-aged rats for examining molecular alterations associated with prostatic Zn loss that might lead to PCa initiation. As shown in the experimental design (Fig. 1*A*), 1-mo-old male Sprague–Dawley rats were fed a Zn-deficient (3–4 ppm Zn) or Zn-sufficient (~60 ppm Zn) diet for 1.5, 4, and 10 mo, forming six groups (n = 10–20 rats per group): Zn-deficient and Zn-sufficient 2.5-mo-old young-adult rats, Zn-deficient and Zn-sufficient 5-mo-old adult rats, and Zn-deficient and Zn-sufficient 11-mo-old middle-aged rats. Zn-deficient rats were fed ad libitum; Zn-sufficient rats were pair-fed with Zn-deficient rats to match their decreased food consumption (35, 36). This Zn-deficient diet mimics marked Zn deficiency in human nutrition (35). In addition, 1-mo-old male Wistar-Unilever rats were similarly fed for 9 mo to form Zn-deficient and Zn-sufficient 10-mo-old middle-aged groups (n = 20 rats per group).

Consistent with previous data (24), testis Zn levels (Zn marker) were ~40% lower in all Zn-deficient age groups (young-adult, adult, and middle-aged) than in the corresponding Zn-sufficient age groups ($P < 0.001$) (Fig. 1*B*). Prostatic Zn levels were similar in young-adult rats fed a Zn-deficient or Zn-sufficient diet for 1.5 mo (Fig. 1*C*). As expected (24), prostatic Zn levels were significantly reduced in Zn-deficient adult as compared with Zn-sufficient adult rats after a 4-mo dietary regimen ($P < 0.001$) (Fig. 1*C*) and in Zn-deficient middle-aged rats relative to their Zn-sufficient counterparts after an ~10-mo regimen in both rat strains [Sprague–Dawley rats, $P < 0.01$ (Fig. 1*C*); Wistar-Unilever rats, $P = 0.025$) (see Fig. 3*D*)]. These results established a middle-aged rat model with prostatic Zn loss induced by a Zn-depleted diet in two rat strains.

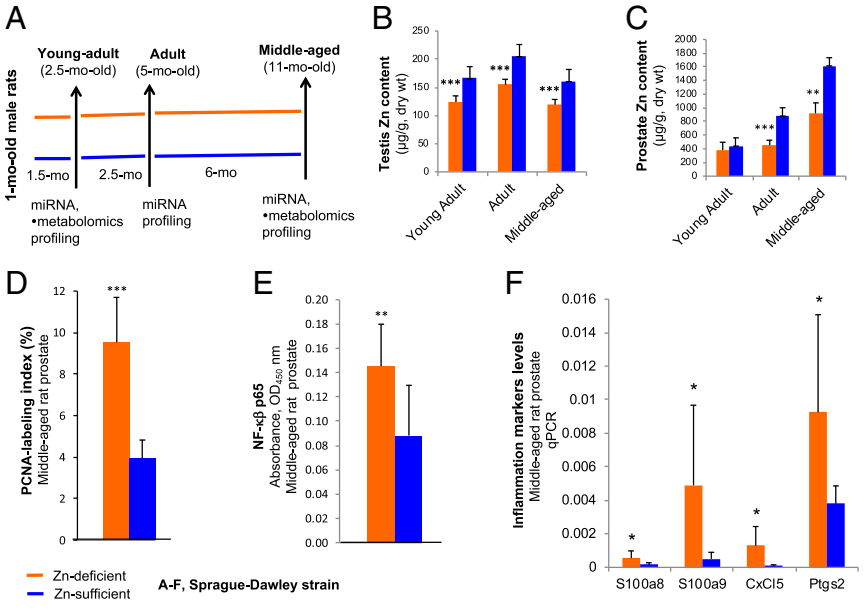

Fig. 1. Establishment of a Zn-deficient middle-aged Sprague–Dawley rat model with prostatic Zn loss. (*A*) Study design: 1-mo-old male rats received a Zn-deficient or Zn-sufficient diet for 1.5, 4, or 10 mo to form six Zn-modulated age groups (n = 10–20 rats per group): Zn-deficient young-adult, adult, and middle-aged and Zn-sufficient young-adult, adult, and middle-aged. (*B* and *C*) Testis Zn content (*B*) and prostate Zn content (*C*) (measured in micrograms per gram dry weight) of young-adult, adult, and middle-aged rats on a Zn-deficient or a Zn-sufficient diet (n = 7–12 rats per group). (*D*) The PCNA-labeling index in middle-aged prostate is expressed as the percent of intensely stained PCNA-positive nuclei (S-phase) per ~500 prostate epithelial nuclei evaluated in a microscope field at 200× magnification (n = 9 rats per group). (*E*) NF-κβ p65 DNA-binding activity of nuclear extracts from middle-aged rat prostates was measured by the TransAM NF-κβ p65 assay kit (n = 9 rats per group). (*F*) qPCR analysis of four selected inflammation genes, *S100a8*, *S100a9*, *Cxcl5*, and *Ptgs2*, in middle-aged rat prostates (n = 6–10 rats per group, measurements were performed in triplicate with Psmb6 as a normalizer). Data are expressed as mean ± SD. All statistics are two-sided; $*P < 0.05$, $**P < 0.01$, $***P < 0.001$.

Zn-Deficient Middle-Aged Rat Prostate Has a Precancerous Phenotype. Histological examination (H&E-stained sections, $n = 10$ rats per dietary group) showed that Zn-sufficient middle-aged rat prostate was typically growth quiescent (37), displaying a thin epithelium (Fig. 2*A*). By contrast, Zn-deficient middle-aged rat prostates displayed frequent epithelial hyperplasia (Fig. 2*A*). To evaluate prostate epithelial cellular proliferation, the proliferation marker proliferating cell nuclear antigen (PCNA) was assessed in formalin-fixed paraffin-embedded (FFPE) rat prostate tissues. PCNA-immunohistochemistry (IHC) showed that the percent of intensely stained PCNA-positive nuclei (S-phase) in Zn-deficient middle-aged prostate (9.5 ± 2.2%) was markedly increased relative to Zn-sufficient middle-aged prostate (3.9 ± 0.9%) ($P < 0.001$; $n = 9$ rats per group) (Figs. 1*D* and 2*A*), indicating that dietary Zn deficiency induces epithelial proliferation in middle-aged rat prostates.

Chronic inflammation is implicated in the pathogenesis of PCa (38), and NF-κβ is a pivotal transcription factor in inflammation (39). The inflammation markers *S100A8/A9* (40), *CXCL5* (41), and *PTGS2* (*COX-2*) (42) are overexpressed in human PCa. An ELISA showed that NF-κβ p65 expression was significantly up-regulated in Zn-deficient middle-aged prostate compared with Zn-sufficient middle-aged prostate ($P < 0.01$; $n = 9$ rats per group) (Fig. 1*E*). qPCR analysis showed that these same four inflammation markers were significantly up-regulated in Zn-deficient middle-aged rats vs. their Zn-sufficient counterparts ($P < 0.05$) (Fig. 1*F*). IHC analysis in FFPE prostate tissues demonstrated that NF-κβ p65 and NF-κβ–regulated COX-2 were strongly expressed in proliferative Zn-deficient as compared with quiescent Zn-sufficient middle-aged rat prostate ($n = 10$ Wistar-Unilever rats per dietary group) (Fig. 2*A*). In addition, IHC analysis of prostatic PCNA and inflammation markers in Zn-deficient 2.5-mo-old young-adult and 11-mo-old middle-aged Sprague–Dawley rats showed that cell proliferation and inflammation progress with aging ($n = 10$ rats per age group) (Fig. 2*B*). Together, the data establish that Zn-deficient middle-aged rat prostates have a hyperplastic and inflammatory phenotype and that the effect of Zn depletion progresses with age.

Overexpression of the Zn-Homeostasis–Regulating miR-183-96-182 Cluster in Zn-Deficient Middle-Aged Rat Prostate. We have shown by nanoString mouse miRNA assay that dietary Zn deficiency for 23 wk in adult rats causes altered miRNA expression in prostate (24). To compare miRNA expression profiles in rats growing from young adult to middle age on a Zn-deficient or Zn-sufficient diet, we employed a nanoString miRNA assay detecting >400 rat miRNAs ($n = 6$ Sprague–Dawley rats per group). The nanoString platform measures miRNA expression levels without reverse transcription or PCR amplification, thus eliminating enzymatic bias (43). Using a cutoff of $P < 0.05$ and a fold-change ≥1.4, 65 dysregulated miRNAs were identified in Zn-deficient middle-aged prostate as compared with Zn-deficient young-adult prostate. Among them, 14 up-regulated and nine down-regulated miRNAs were similarly dysregulated in human PCa (*SI Appendix*, Table S1). The entire miR-183-96-182 cluster that is overexpressed in human PCa (9, 27) and that regulates Zn homeostasis of PCa cells via suppression of Zn transporters [specifically hZIP1 (9)] was up-regulated in Zn-deficient middle-aged rat prostates as compared with young-adult rat prostates (miR-183, up-regulated 1.41-fold, $P = 0.006$; miR-96, up-regulated 2.38-fold, $P = 0.0003$; miR-182, up-regulated 1.73-fold, $P = 0.029$) (Fig. 3*A* and *SI Appendix*, Table S1). By contrast, among the 38 up-regulated miRNAs identified in Zn-sufficient middle-aged rat prostates compared with young-adult rat prostates (*SI Appendix*, Table S2), 11 were identical to those overexpressed in Zn-deficient middle-aged rat prostates and human PCa, including miR-96, a member of the miR-183-96-182

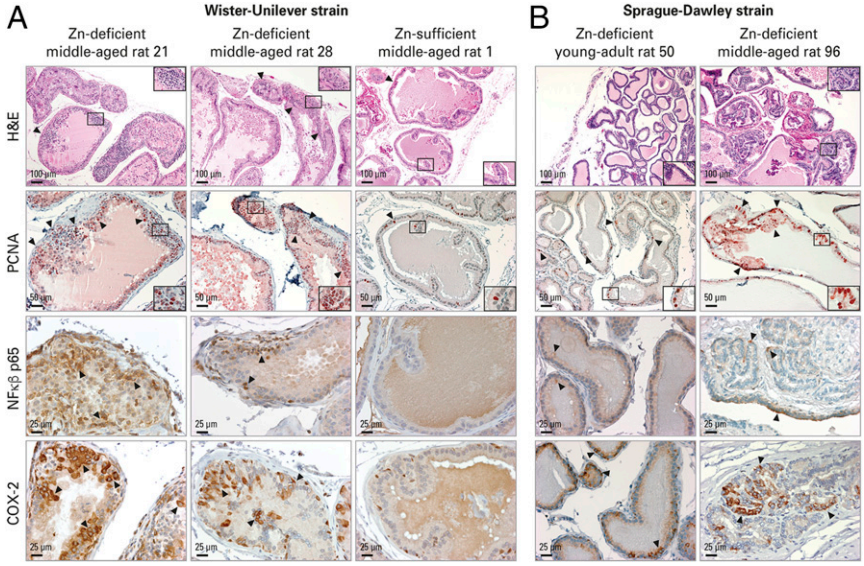

Fig. 2. Zn-deficient middle-aged rat prostate shows increased cellular proliferation and inflammation. H&E analysis of histology and IHC analysis of PCNA, NF-κβ p65, and COX-2 protein expression were performed in FFPE prostate tissues. (*A*) Zn-deficient middle-aged Wistar-Unilever rat prostate vs. Zn-sufficient counterparts ($n = 10$ rats per dietary group). (*Top Row*) H&E-staining shows representative prostates from Zn-deficient middle-aged rats no. 21 and 28 displaying proliferative epithelia (arrowheads) and prostate from Zn-sufficient middle-aged rat 1 showing a thin epithelium (arrowhead) with infolding. (Scale bars: 100 μm in main panels and 50 μm in *Insets*.) (*Second Row*) In PCNA IHC, Zn-deficient middle-aged prostates show abundant PCNA-positive nuclei (red; 3-amino-9-ethylcarbazole substrate-chromogen; arrowheads); Zn-sufficient counterparts display few PCNA-positive nuclei. (Scale bars: 50 μm in main panels and 25 μm in *Insets*.) Additionally, Zn-deficient middle-aged prostates showed strong cytoplasmic NF-κβ p65 (*Third Row*) and intense COX-2 (*Bottom Row*) expression with typical perinuclear cytoplasmic staining; Zn-sufficient middle-aged prostates showed no NF-κβ p65 staining and occasional COX-2–positive staining (brown, DAB). (Scale bars: 25 μm.) (*B*) Compared with Zn-deficient young-adult rat prostate, Zn-deficient middle-aged prostate was proliferative (H&E staining, *Top Row*) (Scale bars: 100 μm in main panels and 50 μm in *Insets*) with frequent PCNA-stained nuclei (*Second Row*) (Scale bars: 50 μm in main panels and 50 μm in *Insets*), moderately strong cytoplasmic NF-κβ p65 expression (*Third Row*) and intense COX-2 expression (*Bottom Row*) (Scale bars: 100 μm).

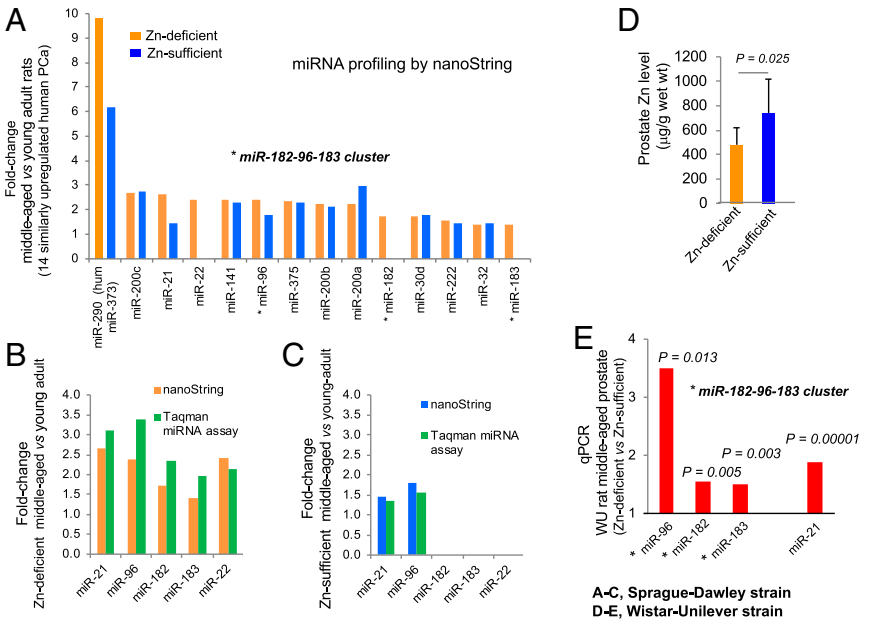

Fig. 3. Prostate miRNA expression profiling by the nanoString nCounter rat miRNA assay in Sprague–Dawley rats (*A*–*C*) and Wistar-Unilever rats (*D* and *E*) growing from young adult into middle age on a Zn-deficient diet or a Zn-sufficient diet. (*A*) Bar plot showing fold-change of 14 miRNAs up-regulated in Zn-deficient middle-aged vs. Zn-deficient young-adult prostates that are similarly up-regulated in human PCa compared with 11 such miRNAs up-regulated in Zn-sufficient middle-aged vs. Zn-sufficient young-adult prostates (cutoff: fold change ≥1.4, $P < 0.05$, $n = 6$ rats per cohort). Asterisks denote up-regulation of the oncogenic miR-183-96-182 cluster. (*B*) Validation of five selected miRNAs (identified by the nanoString platform) in Zn-deficient middle-aged vs. Zn-deficient young-adult rat prostates by the TaqMan miRNA assay (with snoRNA as normalizer, measurements performed in triplicate, $n = 8$ rats per cohort). (*C*) Validation of five selected miRNAs (identified by nanoString platform) in Zn-sufficient middle-aged vs. young-adult rat prostates by the TaqMan miRNA assay (snoRNA as normalizer, measurements performed in triplicate, $n = 8$ rats per cohort). (*D*) Prostate Zn content (measured in micrograms per gram wet weight; mean ± SD, $n = 9$–11 rats per cohort). (*E*) Expression of the miR-183-96-182 cluster and miR-21 in prostates of Zn-deficient middle-aged Wistar-Unilever rats (qPCR, snoRNA as normalizer, assays performed in triplicate, $n = 9$–12 rats per group). Data are expressed as fold-change in Zn-deficient vs. Zn-sufficient middle-aged rat prostates. All statistics are two-sided.

cluster (Fig. 3*A*). These results indicate that Zn deficiency is necessary for the expression of the entire cluster. Additionally, miRNA profiling in adult and young-adult prostate revealed that while two members of the miR-183-96-182 cluster, miR-183 and mir-96, were detected in Zn-deficient adult vs. young-adult prostate (*SI Appendix*, Table S3), none was found in Zn-sufficient adult vs. young-adult prostate (*SI Appendix*, Table S4). Thus, up-regulation of the entire miR-183-96-182 cluster in rat requires Zn-deficient, middle-aged prostate.

Using TaqMan miRNA assays [$n = 8$ rats per cohort, small nucleolar RNA (snoRNA) as normalizer], we validated the nanoString results of five selected miRNAs (the miR-183-96-182 cluster, miR-21, and miR-22) in Zn-deficient middle-aged vs. Zn-deficient young prostates (Fig. 3*B*) and of miR-96 and miR-21 up-regulation in Zn-sufficient middle-aged vs. Zn-sufficient young prostates (Fig. 3*C*).

Consistent with the results in the Sprague–Dawley strain, prostates of Zn-deficient middle-aged Wistar-Unilever rats that exhibited prostatic Zn decline relative to their Zn-sufficient counterparts ($P = 0.025$) (Fig. 3*D*) also showed statistically significant up-regulation of the entire miR-183-96-182 cluster (miR-183, up-regulated 1.51-fold, $P = 0.003$; miR-96, up-regulated 3.50-fold, $P = 0.013$; miR-182, up-regulated 1.54-fold, $P = 0.005$) (Fig. 3*E*) and miR-21, an inflammation-associated oncomiR (44) (up-regulated 1.89-fold, $P = 0.0001$) (Fig. 3*E*).

Zn Importer and Zn Exporter Expression Profiles in Zn-Deficient Middle-Aged Rat Prostate Resemble Profiles in Human PCa. Zn homeostasis is maintained mainly by two families of Zn transporters with opposing roles (45). Whereas Zn importers (Zip) in the SLC39 Zn transporter family bring Zn into the cytoplasm from the extracellular space, Zn exporters (ZnT) in the SLC30 Zn transporter family remove Zn from the cytoplasm and transport it into cellular organelles. There are 24 known Zn transporters (Zip 1–14 and ZnT 1–10). Consistent with the loss of the ability to accumulate Zn, human PCa tissue showed down-regulation of hZIP1 (7–9), hZIP2 and hZIP3 (10), and hZIP14 (46), and, perhaps not incidentally, the high incidence of PCa in African Americans vs. white Americans is associated with the down-regulation of hZIP1 and hZIP2 (8). The role of Zn exporters in PCa has not been defined, but significant up-regulation of ZnT1, ZnT9, and ZnT10 expression and down-regulation of ZnT6 and ZnT5 expression were reported in PCa (47).

To investigate the involvement of Zn transporters in prostatic Zn decline in Zn-deficient middle-aged rats, qPCR was used to analyze the expression of 14 Zn importers (Zip1–14) and 10 Zn exporters (ZnT1–10) ($n = 9$–11 Wistar-Unilever rats per cohort). We found that the Zn-depleted middle-aged prostate displayed a Zip expression profile mimicking that of human PCa (7–10, 46), with statistically significant down-regulation of multiple Zips, including Zip1 ($P = 0.0019$), Zip2 ($P = 0.026$), Zip3 ($P = 0.0012$), and Zip14 ($P = 0.042$) (Fig. 4*A*). Among Zn exporters, the ZnT expression profile of Zn-deficient middle-aged prostate showed up-regulation of ZnT1, ZnT9, and ZnT10 and down-regulation of ZnT6 ($P < 0.05$) (Fig. 4*B*), again resembling profiles of human PCa (47).

Inverse Relationship Between the miR-183-96-182 Cluster and ZIP1 in Zn-Deficient Middle-Aged Rat Prostate. We focused on Zip1, a bona fide target of miR-182 (9). The Zip1 mRNA level was down-regulated 1.97-fold ($P = 0.0019$) (Fig. 4*A*) in Zn-deficient middle-aged Wistar-Unilever rat prostate that documented up-regulation of the entire oncogenic miR-183-96-182 cluster (miR-182, up-regulated 1.54-fold, $P = 0.005$) (Fig. 3*E*). Using in situ hybridization (ISH) for localization of miR-182 and IHC for

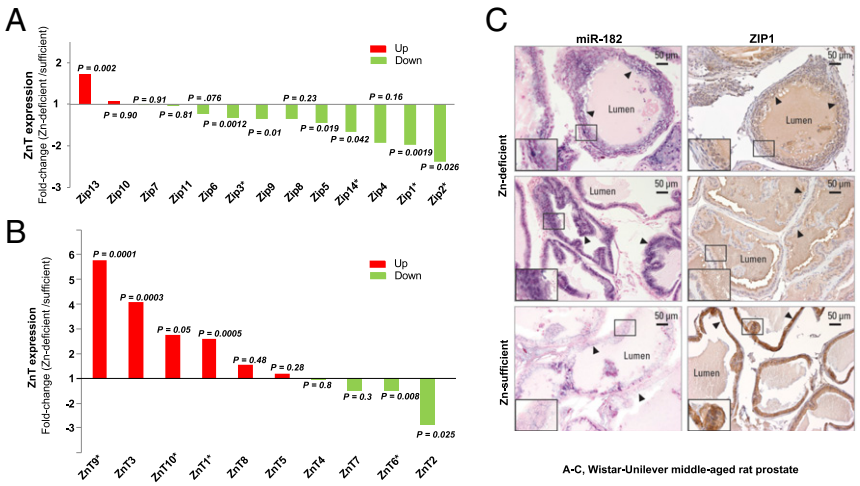

Fig. 4. Zip and ZnT expression profiles of Zn-deficient middle-aged rat prostates resemble profiles of human prostate cancer and the relationship between miR-182 up-regulation and ZIP1 mRNA/protein down-regulation. (*A* and *B*) qPCR analyses of Zn importers (Zip 1–14; Zip12 is not detectable) (*A*) and Zn exporters (ZnT 1–10) (*B*) in prostates from Zn-deficient vs. Zn-sufficient middle-aged Wistar-Unilever rats (Oaz1 as normalizer, measurements performed in triplicate, n = 9–11 rats per cohort; two-sided t test). Asterisks denote Zip and ZnT expression similarly up- or down-regulated in human prostate cancer. (*C*) ISH cellular localization of miR-182 by mmu-miR-182 detection probe (double digoxigenin-labeled at the 5′ and 3′ ends) and IHC analysis of ZIP1 protein expression in FFPE prostate tissues of Zn-deficient vs. Zn-sufficient middle-aged rat prostates. Intense/frequent miR-182 ISH signal (blue) was detected in Zn-deficient middle-aged prostate (two representative samples are shown) vs. very weak and diffuse miR-182 ISH signals (blue) in Zn-sufficient middle-aged prostate (blue, 4-nitro-blue tetrazolium and 5-bromo-4-chloro-3′-indolyl phosphate counterstained by nuclear fast red). ZIP1 protein expression was diffuse and weak (brown staining, DAB) in representative ZN-deficient middle-aged rat prostate epithelia vs. strong ZIP1 expression (brown staining) in epithelial cells of a Zn-sufficient middle-aged rat prostate. n = 10 rats per group. (Scale bars: 50 μm in main panels and 25 μm in *Insets*.)

ZIP1 protein expression, we found that proliferative Zn-deficient middle-aged Wistar-Unilever prostate epithelia displayed intense, abundant miR-182 signals (blue stained in Fig. 4*C*) and diffuse and weak immunostaining of ZIP1 protein (brown stained in Fig. 4*C*), demonstrating that up-regulation of miR-182 represses Zip1 gene expression by inhibiting its translation into protein. Conversely, nonproliferative Zn-sufficient middle-aged Wistar-Unilever prostate epithelia displayed weak to absent miR-182 signals and resultant strong ZIP1 protein expression (Fig. 4*C*). Thus, dietary Zn deficiency induces up-regulation of the miR-183-96-182 cluster, leading to the suppression of Zip1 (a target of miR-182) and thereby reducing prostatic Zn accumulation.

Inverse Relationship Between miR-182 and hZIP1 in Human Prostate Adenocarcinoma Tissue. We next evaluated the relationship between miR-182 and hZIP1 in human PCa. Using archival prostate adenocarcinoma FFPE tissue and paired adjacent nonneoplastic prostate, we performed untargeted miRNA expression profiling by the nanoString human miRNA assay (n = 4 paired samples). miRNA analysis showed that among the 12 up-regulated miRNAs with fold-change >1.6 (hsa-miR-182-5p, -375, -19a-3p, -582-5p,

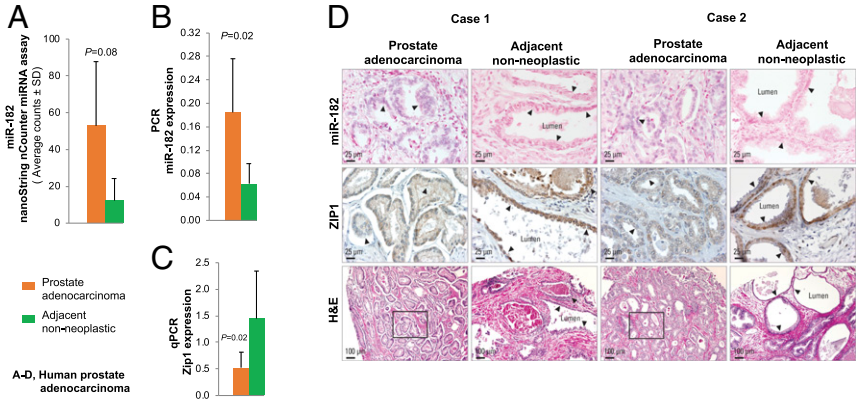

Fig. 5. Human prostate adenocarcinoma tissue shows an inverse relationship between miR-182 up-regulation and hZIP1 down-regulation. (*A*) A nanoString nCounter human miRNA assay showing miR-182 up-regulation in human prostate adenocarcinoma vs. adjacent nonneoplastic prostate (n = 4 paired samples; P = 0.08). (*B*) qPCR validation of the miR-182 result by nanoString (TaqMan miRNA assay, hsa-miR-182-5p, RNU44 as normalizer, measurements performed in triplicate, n = 6 paired samples; P = 0.02). (*C*) qPCR analysis showing hZIP1 down-regulation in human prostate adenocarcinomas vs. adjacent nonneoplastic prostate (OAZ1 as normalizer, measurements performed in triplicate; n = 6 paired samples; P = 0.02). Data are expressed as mean ± SD. (*D*) ISH cellular localization of miR-182 using the hsa-miR-182 detection probe (double digoxigenin-labeled at the 5′ and 3′ ends) and IHC analysis of hZIP1 protein expression (n = 6 paired human prostate adenocarcinomas and adjacent prostate tissue). Representative patient cases 1 and 2 show moderate/frequent miR-182 ISH signals (blue, 4-nitro-blue tetrazolium and 5-bromo-4-chloro-3′-indolyl phosphate; nuclear fast red counterstain) in prostate adenocarcinoma but no miR-182 ISH signals in adjacent nonneoplastic prostate tissue. hZIP1 immunostaining was diffuse and weak (brown, DAB) in prostate adenocarcinoma but was strong in nonneoplastic prostate epithelial cells.

-378e, -200c-3p, -148a-3p, -93-5p, -20a-5p, -141-3p, -30b-5p, and -96-5p), miR-182 was the top up-regulated species (up-regulated 4.3-fold, $P = 0.08$, $n = 4$ paired samples) (Fig. 5*A*). Using TaqMan miRNA assays of six FFPE-derived normal and tumor RNA pairs, we validated the nanoString results. The miR-182 level was statistically significantly up-regulated in prostate adenocarcinoma relative to adjacent nonneoplastic prostate ($P = 0.02$; RNU44 as normalizer) (Fig. 5*B*). In parallel, qPCR analysis showed statistically significant down-regulation of hZIP1 in these prostate adenocarcinoma tissues vs. adjacent nonneoplastic prostate pairs ($P = 0.02$; OAZ1 as normalizer, $n = 6$ paired samples) (Fig. 5*C*). We then conducted ISH for miR-182 cellular localization and IHC for hZIP1 protein expression in FFPE prostate adenocarcinoma and adjacent prostate tissue ($n = 6$ paired patient cases) (representative cases 1 and 2 are shown in Fig. 5*D*). We demonstrated the same inverse relationship between miR-182 up-regulation and hZIP1 down-regulation in human prostate adenocarcinoma (Fig. 5*D*) as in Zn-deficient middle-aged rat prostate (Fig. 4*C*). Although the Zn status in these human PCa tissues was not measured, this finding is consistent with the premise that prostatic Zn loss is a characteristic of PCa.

Zn-Deficient Middle-Aged Rat Prostate Exhibits a Human PCa-Like Metabolic Phenotype. Normal human prostate cells accumulate Zn that inhibits citrate oxidation. Conversely, PCa cells with prostatic Zn loss actively oxidize citrate, leading to a reduction in citrate synthesis (29). Metabolic reprogramming is a hallmark of cancer (48), including prostate cancers (31, 32). Cancer metabolism alters cellular metabolic phenotypes to sustain tumor growth. In addition, some primary metabolites such as 2-hydroxyglutarate directly impact cellular regulation through epigenetic alteration (49). Accordingly, we focused on primary metabolism to detail metabolic phenotypes in Zn-depleted middle-aged prostate tissue and Zn-sufficient counterparts, using a long-established untargeted metabolomics platform, GC-TOF-MS. GC-TOF-MS has been used in the study of metabolic reprogramming in multiple human cancers, including ovarian carcinoma (50) and lung adenocarcinoma (51).

Our metabolomics analysis yielded 599 compounds ($n = 9$ Wistar-Unilever rats per group), of which we structurally identified 175 unique metabolites. A total of 18 statistically significantly altered metabolites were identified in Zn-deficient vs. Zn-sufficient middle-aged rat prostate (Table 1). Citric acid itself was prominently down-regulated (10-fold, $P = 0.0003$), mimicking the down-regulation in human PCa (31, 32). By contrast, Zn-deficient young-adult prostate tissue that did not show evidence of Zn loss (Fig. 1*C*) had no metabolic changes in citrate content (*SI Appendix*, Table S5). To obtain a biochemical overview of classic univariate statistics differences between Zn-depleted and Zn-sufficient middle-aged rat prostates, we constructed a metabolomic network (52) that combined biochemical relationships through the Kyoto Encyclopedia of Genes and Genomes (KEGG) database annotations of metabolic substrate/product reaction pairs (53) and chemical similarities through Tanimoto substructure matrix analysis from PubChem compound identifiers (Fig. 6*C*) (54). This network analysis showed that only the citrate-dependent part of the TCA cycle (i.e., citrate, aconitate, and isocitrate) but not subsequent TCA metabolites (including the TCA oxidation products 2-oxoglutarate and succinate) was down-regulated in Zn-deficient as compared with Zn-sufficient middle-aged prostate. This finding supports the conclusion that the Zn-deficient rat prostate TCA cycle is supported by anaplerotic influx of carbon, likely through glutaminase. The metabolic network (Fig. 6*C*) further highlights a decrease in purine nucleosides inosine and guanosine concomitant with a 1.23-fold increase in the pyrimidine nucleobase uracil ($P = 0.040$) (Fig. 6 *B* and *C*). This increase in uracil (55) may indicate a chokepoint in prostate metabolism (56) replacing the well-known cancer metabolic chokepoint pyruvate dehydrogenase (Warburg effect) in prostate cancers. Glycogen metabolism was decreased, as indicated by lower levels of glucose-1-phosphate and maltose (a glycogen degradation product) (Fig. 6*C*). These data establish that

Table 1. Human prostate cancer metabolic phenotype in Zn-deficient middle-aged rat prostate

Metabolite	Median fold-change in Zn-deficient vs. Zn-sufficient middle-aged rat prostate	*P* value	Biological process
Down-regulated			
Citric acid*	−10.14	0.0003	TCA
Isocitric acid	−4.62	0.0012	TCA
Aconitic acid	−2.58	0.0003	TCA
Glycerol-alpha phosphate	−2.08	0.0188	Carbon metabolism
Guanosine	−2.05	0.0188	Purine metabolism
Glucose-1-phosphate	−1.82	0.0012	Glycolysis/gluconeogenesis
Squalene	−1.52	0.0400	Steroid biosynthesis
Inosine	−1.46	0.0244	Purine metabolism
Maltose	−1.37	0.0188	Starch and sucrose metabolism
Up-regulated			
Salicylaldehyde	1.89	0.0106	—
Fructose-1-phosphate	1.83	0.0028	Fructose and mannose metabolism
Arabinose	1.65	0.0078	—
Tyrosine	1.58	0.0078	Tyrosine metabolism
Ribose	1.48	0.0188	Pentose phosphate pathway
Inositol-4-monophosphate	1.40	0.0142	Inositol phosphate metabolism
Capric acid	1.35	0.0244	Fatty acid biosynthesis
Lauric acid	1.29	0.0244	Fatty acid metabolism
Uracil*	1.23	0.0400	Pyrimidine metabolism

Untargeted metabolomics profiling by GC-TOF-MS was performed in Zn-deficient 10-mo-old middle-aged Wistar-Unilever rat prostate and Zn-sufficient middle-aged rat prostate ($n = 9$ rats per group). A signature of 18 metabolites was significantly dysregulated in Zn-deficient vs. Zn-sufficient middle-aged rat prostate ($P < 0.05$).
*Citric acid and uracil are similarly dysregulated in human prostate cancer.

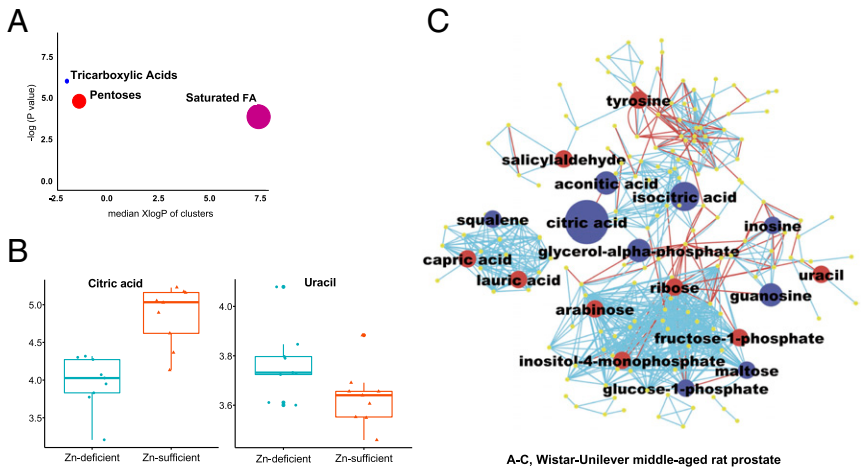

Fig. 6. Untargeted metabolomics profiling by GC-TOF-MS reveals a human PCa-associated metabolic phenotype in Zn-deficient middle-aged Wistar-Unilever rat prostates with marked down-regulation of citrate ($n = 9$ rats per group). (*A*) ChemRICH set enrichment statistics plot showing that TCA metabolites were down-regulated in Zn-deficient middle-aged vs. Zn-sufficient middle-aged rat prostates, with pentose metabolites and saturated fatty acids up-regulated. The node color scale shows the proportion of increased (red) or decreased (blue) compounds in Zn-deficient vs. Zn-sufficient middle-aged prostate. Purple nodes have both increased and decreased metabolites. (*B*) Box-and-whisker plots (data log10 transformed) for citric acid and uracil (two metabolites similarly dysregulated in human PCa) in the Zn-deficient and Zn-sufficient middle-aged rat prostates. (*C*) Metabolomics network of biochemical differences between Zn-deficient and Zn-sufficient middle-aged rat prostates. A biochemical and chemical similarity network was calculated for all measured metabolites with KEGG and PubChem CIDs. Molecules not directly participating in biochemical transformations but sharing many structural properties were connected at a threshold of Tanimoto similarity coefficient ≥0.7. Each node denotes an identified metabolite (blue, down-regulated; red, up-regulated; yellow, insignificant change; $P < 0.05$; Mann–Whitney *U* test). Metabolites are connected based on biochemical relationships (red lines) or structural similarity (light-blue lines). Metabolite size reflects median fold-change.

the Zn-depleted middle-aged rat prostate exhibits a specific, human PCa-related metabolic phenotype.

Finally, to establish a statistical assessment of a differential regulation of full metabolic modules, we employed chemical set enrichment statistics (ChemRICH) (*SI Appendix*, Table S6) (57). Unlike pathway enrichment statistics, ChemRICH uses non-overlapping groups of metabolites based on chemical similarity and ontology mapping. ChemRICH tests statistical significance using the Kolmogorov–Smirnov test that is not dependent on the size of background databases (57). This analysis showed that pentoses, notably the key members arabinose and ribose (Fig. 6*C*), were significantly up-regulated (Fig. 6*A* and *SI Appendix*, Table S7) and also showed differential regulation of medium-chain saturated fatty acids (Fig. 6 *A* and *C*). In combination, these results show details of the overall reprogramming of prostate cell metabolism under Zn-deficient conditions, highlighting specific parts of dysregulated metabolic modules.

Discussion

Prostatic Zn decline in the malignant cells is a consistent characteristic of prostate cancer, with unknown causes and consequences that could be properly and thoroughly investigated only in an animal model. We believe that the animal model we describe has confirmed this association between dietary Zn and prostate cancer risk and has established the mechanisms underlying the link. With a low-Zn diet, this Zn-deficient middle-aged rat prostate model shows prostatic Zn loss and inflammation. To uncover the molecular changes associated with Zn loss, we did a complete miRNA expression profile, Zn transporter expression profiles, and a metabolome profile in Zn-deficient middle-aged vs. Zn-sufficient middle-aged prostate. We found a mechanistic link that ties dietary Zn deficiency to prostatic Zn loss. This result is highly significant, since how dietary Zn intake influences prostate Zn content had not been previously known. In outline, our findings show that Zn deficiency up-regulates the expression of the miR-183-96-182 cluster in hyperplastic/inflammatory Zn-deficient middle-aged prostate with resultant ZIP1 down-regulation to reduce prostate Zn and an outcome leading to citrate down-regulation, a hallmark of the human prostate cancer metabolome.

The miR-183-96-182 cluster is overexpressed in human PCa and regulates Zn homeostasis in PCa cells (9). Thus, the finding that this same miRNA cluster is overexpressed in Zn-deficient middle-aged prostates is compelling and emphasizes the relevance of this model in defining the molecular consequences of prostatic Zn decline in prostate neoplasia. Consistent with the role of this miRNA cluster in Zn homeostasis, Zn-depleted middle-aged prostate displayed a Zn importer profile resembling that of human PCa tissue (7–10, 46), with down-regulation of multiple Zip importer genes: *Zip1*, *Zip2*, *Zip3*, and *Zip14* (Fig. 4*A*). This inverse relationship of miR-182 overexpression with its target ZIP1 protein down-regulation was visualized and confirmed in FFPE tissue sections of Zn-deficient middle-aged rat prostate (Fig. 4*C*) as well as in human prostate adenocarcinoma tissue (Fig. 5*D*), with results indicating that miR-182 overexpression represses *Zip1* gene expression by inhibiting its translation into protein. The data provide a mechanism explaining how dietary Zn insufficiency leads to Zn loss in the middle-aged prostate.

It is established that normal human prostate epithelial cells have a Zn-accumulating and citrate-synthesizing phenotype (30). By contrast, PCa cells reorder this phenotype and take on a Zn-diminishing and citrate-oxidizing phenotype (29). The Zn-deficient young-adult prostates that retain the ability to accumulate Zn (Fig. 1*C*) show no changes in citrate levels (*SI Appendix*, Table S5). In Zn-deficient middle-aged prostates that lose ability to accumulate Zn, citrate is decreased along with isocitrate and aconitate but not the other metabolites of the TCA cycle (Fig. 6*C* and Table 1), thereby confirming that reduction of citrate level is indeed a distinct metabolic phenotype resembling the human prostate cancer phenotype (31, 32). These in vivo results establish a direct link between dietary Zn deficiency, prostatic Zn loss, and resultant citrate down-regulation, changes that mimic features of human PCa.

Because of inconsistent epidemiologic data regarding dietary Zn and PCa risk and the lack of relevant animal models, the relationship between Zn and prostate health remains an unresolved "critical scientific, medical, and public interest issue" (58). Our in vivo findings in prostate tissue of middle-aged rats, with similarity to observations of PCa in middle-aged men, have revealed a mechanistic link between low dietary Zn and features of human PCa that include miR-183-96-182 overexpression, ensuing ZIP1 down-regulation, Zn decline, and citrate reduction. Thus, the data indicate that dietary Zn insufficiency can increase the risk of prostate cancer.

Given that human populations are mostly mildly to moderately Zn insufficient (12), a limitation of this study is the use of a low-Zn diet to represent marked Zn deficiency in human nutrition (35). Future studies in aging rats are needed to investigate the dose–response relationship between the level of dietary Zn deficiency and the level of prostatic Zn decline and associated molecular alterations. Studies are also needed to determine whether dietary Zn insufficiency promotes not only prostate preneoplasia but also progression to prostate cancer and, particularly, whether Zn supplementation could reverse the process.

Materials and Methods

Rat Studies. We used two rat strains, the Sprague–Dawley (Taconic) and Wistar-Unilever (HsdCpb:Wu) (Envigo) strains, and custom-formulated Zn-deficient (3–4 ppm Zn) and Zn-sufficient (~60 ppm Zn) diets from Harlan Teklad. Briefly, 1-mo-old male Sprague–Dawley rats were fed a Zn-deficient or Zn-sufficient diet for 1.5, 4, or 10 mo to form six Zn-modulated age groups (n = 10–20 rats per group): Zn-deficient young-adult, adult, and middle-aged groups and Zn-sufficient young-adult, adult, and middle-aged groups. Additionally, 1-mo-old male Wistar-Unilever rats were similarly fed for 9 mo to form Zn-deficient and Zn-sufficient middle-aged groups (n = 20 rats per group). Zn-deficient rats were fed ad libitum; Zn-sufficient rats were pair-fed with Zn-deficient rats to match their decreased food consumption (35, 36). The rats were housed six to a stainless-steel cage and were given deionized drinking water. Zn-modulated young-adult, adult, and middle-aged rats were killed at age 2.5 mo, 5 mo, and 9–10 mo, respectively. Testis and lateral prostate were isolated. All animal protocols were approved by the Thomas Jefferson University Animal Care and Use Committee.

Prostate Isolation. Animals were anesthetized by delivering isoflurane (GE Healthcare) to the respiratory tract of the rat using a vaporizer at 3% concentration. The testis and the genitourinary tract comprising the bladder, urethra, seminal vesicles, and ampullary gland were excised. The prostate was microdissected into individual lobes, and the lateral prostate was isolated and was cut into two portions. One portion was snap-frozen in liquid nitrogen and stored at −80 °C. The remaining prostate portion was fixed in 10% buffered formalin and was paraffin embedded. Testis was stored at 4 °C.

Zn Measurement. Samples of testis and prostate were dried to constant weight at 90 °C and then were ashed in a furnace. Ashed samples were dissolved in 0.1 M HCl solution. Tissue Zn content was determined by atomic absorption spectrometry using AAnalyst 400 (Perkin-Elmer).

RNA Extraction. Lateral prostate samples frozen in liquid nitrogen were pulverized to a fine powder using a chilled hammer. Total RNA was extracted from the pulverized samples using an animal tissue RNA extraction kit (no. 25700; Norgen Biotek). The RNA concentration of each sample was determined using a NanoDrop 1000 spectrophotometer (Thermo Scientific). All RNA samples displayed a 260:280 ratio >1.8, and a 260:230 ratio >1.8.

Human Prostate Adenocarcinoma and Paired Nonneoplastic Prostate Tissue. Sixteen FFPE archival prostate adenocarcinoma samples and paired nonneoplastic tissue (Pathology Department, Thomas Jefferson Hospital, Philadelphia) were selected from eight anonymized cases for which patient-related information was unavailable.

NanoString Rat miRNA Expression Assay. This miRNA expression assay kit profiles 423 rat miRNAs. This assay was performed at the Ohio State University Comprehensive Cancer Center Genomics Shared Resource according to the manufacturer's instructions (n = 6 rats per group). Briefly, 100 ng of total RNA was used as input material. Small RNA samples were prepared by ligating a specific DNA tag onto the 3′ end of each mature miRNA. These tags normalized the melting temperatures of the miRNAs and provided identification for each miRNA species in the sample. Excess tags were then removed, and the resulting material was hybridized with a panel of miRNA: tag-specific nCounter capture and barcoded reporter probes. Hybridization reactions were incubated at 64 °C for 18 h. Hybridized probes were purified and immobilized on a streptavidin-coated cartridge using the nCounter Prep Station. An nCounter Digital Analyzer was used to count individual fluorescent barcodes and quantify target RNA molecules present in each sample. For each assay, a high-density scan (600 fields of view) was performed.

Human miRNA Expression Assay. A human miRNA expression assay detecting >800 human miRNAs (n = 4 paired human prostate adenocarcinoma tissues and adjacent normal prostate tissues) was performed at the Genomic Pathology Laboratory of Thomas Jefferson University Hospitals as described above.

NanoString Data Analysis. Abundances of miRNAs were quantified using the nanoString nCounter gene-expression system (43). Each sample was normalized using the global sum method that uses the entire miRNA content. The nanoString nSolver software tool was used to facilitate normalization. Student's t test was used to calculate statistical significances of pairwise comparisons. Calculations were performed using the R statistical computing environment (https://www.r-project.org/http://www.r-project.org/).

TaqMan miRNA Assay. Reverse transcription of miRNAs was performed according to the manufacturer's instructions (Applied Biosystems) with a reaction volume of 15 μL containing 350 ng of total RNA. Each miRNA and endogenous control (snoRNA and U87) was measured in triplicate. As an overall quality control, cycle threshold (Ct) values above 35 were excluded from analysis. Real-time qPCR was performed using the StepOnePlus Real-time System (Applied Biosystems). The following TaqMan miRNA assays were used: rno-miR-182 (ID no. 002599); hsa-miR-182-5p (ID no. 002334); rno-miR-183-5p (rno481330_mir); mmu-miR-96 (ID no. 000186); rno-miR-21-5p (ID no. 000397); and rno-miR-22-3p (ID no. 000398).

ISH. Double digoxigenin-labeled (5′ and 3′ends) miRCURY LNA mmu-miR-182 and hsa-miR-182 were from Exiqon. ISH was performed on 6-μm FFPE sections as previously described (36). Following deparaffinization, rehydration in graded alcohol, and proteinase K treatment, tissue sections were hybridized with the miR-182 probe (25 nM) in hybridization buffer (Exiqon) at 55 °C for 14 h in a hybridizer (Dako). Following stringent washes in SSC buffers, the sections were blocked against unspecific binding of the detecting antibody, using the DIG Wash and Block Buffer Set (Sigma-Aldrich). The miR-31 ISH signal (blue) was localized by incubation with 4-nitro-blue tetrazolium and 5-bromo-4-chloro-3′-indolyl phosphate (Roche), with nuclear fast red (Vector Lab) as a counterstain.

IHC. IHC on FFPE sections was performed as previously described (36). Tissue sections were incubated with primary antibodies for mouse monoclonal PCNA (dilution 1:300, clone PC-10, Ab-1; Thermo Scientific), rabbit polyclonal NF-κB p65 (dilution 1:500, ab7970; Abcam), rabbit polyclonal COX-2 (dilution 1:300, NB1-689; Novus Biologicals), and rabbit polyclonal SLC39A1 (ZIP1) (dilution 1:2,000, NBP1-76498; Novus Biologicals), followed by incubation with appropriate biotinylated secondary antibodies and streptavidin HRP. Protein was localized by incubation with 3-amino-9-ethylcarbazole substrate-chromogen (Dako) or 3,3′-diaminobenzidine tetrahydrochloride (DAB) (Sigma-Aldrich).

ELISA. Prostate whole-cell extracts were prepared using a nuclear extract kit (Active Motif). NF-κB p65 was quantified using ELISA system (40096; Active Motif).

qRT-PCR. cDNA was reverse transcribed using the High-Capacity cDNA Archive Kit (Applied Biosystems) according to the manufacturer's protocol. qPCR was performed using single-tube TaqMan gene-expression assays (Applied Biosystems) and the Ct method. Each mRNA and normalizer (Psmb6 and Oaz1) was measured in triplicate. As an overall quality control, Ct values above 35 were excluded from analysis. Real-time qPCR was performed using the StepOnePlus Real-time System (Applied Biosystems).

Zn Transporters. We used the following Zip (Slc39a 1–14) and ZnT (Slc30a 1–10) single-tube TaqMan gene-expression assays (Life Technologies): SLC39A1 (Hs00205358_m1), Slc39a1 (Rn01458936_g1), Slc39a2 (Rn01414621_g1), Slc39a3

(Rn01408567_m1), Slc39a4 (Rn01505595_g1), Slc39a5 (Rn01527167_m1), Slc39a6 (Rn01405813_m1), Slc39a7 (Rn01428651_g1), Slc39a8 (Rn01748352_m1), Slc39a9 (Rn01517485_m1), Slc39a10 (Rn01771487_m1), Slc39a11 (Rn01466375_m1), Slc39a12 (Rn01487123_m1), Slc39a13 (Rn01485759_m1), and Slc39a14 (Rn01468336_m1); Slc30a1 (Rn00575737_m1), Slc30a2 (Rn00563633_m1), Slc30a3 (Rn01472608_m1); Slc30a4 (Rn00597094_m1); Slc30a5 (Rn01493867_m1); Slc30a6 (Rn01472405_m1); Slc30a7 (Rn01518625_m1); Slc30a8 (Rn00555793_m1); Slc30a9 (Rn01772805_m1), and Slc30a10 (Rn01412215_m1).

Metabolomics Profiling by GC-TOF-MS. Frozen rat lateral prostates were shipped to the NIH West Coast Metabolomics Center (University of California, Davis) and were processed as described (50).

GC-TOF-MS Data Acquisition and Processing. Prostate tissue ($n = 8$ or 9 rats per cohort; 20 mg per prostate) was extracted and derivatized as described (50). For primary metabolites analysis by GC-TOF-MS, the cold injection/automatic liner exchange (CIS-ALEX) GC-TOF-MS (Leco Pegasus IV) was employed using chromatographic and mass spectrometric parameters. From ∼800 individual peaks detected per chromatogram, 176 identified and 423 unknown genuine metabolites remained after extensive cleanup and filtering through the BinBase metabolomic database (O.F. laboratory, University of California, Davis). Using the FiehnLib libraries (http://mona.fiehnlab.ucdavis.edu/downloads) of over 1,200 mass spectra and retention indices for identified metabolites, structurally known compounds were identified by matching mass spectra and retention indices to authentic standards [Metabolomics Standards Initiative (MSI) level 1 identifications] or were annotated by very high mass spectral similarities to the NIST14 library and close retention time predictions (MSI level 2 identifications; name followed by the label "NIST" in the *SI Appendix*, Table S6). A quality-control sample for extracts was prepared by mixing a small amount (∼5 μL) of biofluid of each sample in a study set, thus providing a sample with the true representation of the breadth of metabolites present in the sample set.

ChemRICH Analysis. ChemRICH analysis was performed on the metabolomics dataset as described (57).

Metabolome Network Visualization. A biochemical and chemical similarity network (52) was calculated for all measured metabolites with KEGG and PubChem identifiers (CIDs).

Statistical Analysis. Student's *t* test and paired Student's *t* test were used to detect differences involving two groups and in paired human samples, respectively. The Mann–Whitney *U* test was used to detect significant compounds in metabolomics. All statistical tests were two-sided and were considered significant at $P < 0.05$. Statistical analysis was performed by R (https://www.R-project.org).

ACKNOWLEDGMENTS. We thank Timothy Flanagan of Medical Media Services, Thomas Jefferson University, for assistance with figure preparation. This work was supported by NIH Grants R01CA118560 (to L.Y.F.) and R35CA197706 (to C.M.C.), NIH West Coast Metabolomics Center Grant U24 DK097154 (to O.F.), and funds from the Department of Pathology, Anatomy and Cell Biology, Thomas Jefferson University.

1. Yatani R, et al. (1982) Geographic pathology of latent prostatic carcinoma. *Int J Cancer* 29:611–616.
2. Gann PH (2002) Risk factors for prostate cancer. *Rev Urol* 4(Suppl 5):S3–S10.
3. Mawson CA, Fischer MI (1952) The occurrence of zinc in the human prostate gland. *Can J Med Sci* 30:336–339.
4. Zaichick VYe, Sviridova TV, Zaichick SV (1997) Zinc in the human prostate gland: Normal, hyperplastic and cancerous. *Int Urol Nephrol* 29:565–574.
5. Costello LC, Franklin RB (2017) Decreased zinc in the development and progression of malignancy: An important common relationship and potential for prevention and treatment of carcinomas. *Expert Opin Ther Targets* 21:51–66.
6. Habib FK, Mason MK, Smith PH, Stitch SR (1979) Cancer of the prostate: Early diagnosis by zinc and hormone analysis? *Br J Cancer* 39:700–704.
7. Franklin RB, et al. (2005) hZIP1 zinc uptake transporter down regulation and zinc depletion in prostate cancer. *Mol Cancer* 4:32.
8. Rishi I, et al. (2003) Prostate cancer in African American men is associated with downregulation of zinc transporters. *Appl Immunohistochem Mol Morphol* 11: 253–260.
9. Mihelich BL, et al. (2011) miR-183-96-182 cluster is overexpressed in prostate tissue and regulates zinc homeostasis in prostate cells. *J Biol Chem* 286:44503–44511.
10. Desouki MM, Geradts J, Milon B, Franklin RB, Costello LC (2007) hZip2 and hZip3 zinc transporters are down regulated in human prostate adenocarcinomatous glands. *Mol Cancer* 6:37.
11. Caulfield LE, Black RE (2004) Zinc deficiency. *Comparative Quantification of Health Risk*, eds Ezzati M, Lopez AD, Rodgers A, Murray CJ (World Health Organization, Geneva), Vol 1, pp 257–280.
12. Maret W, Sandstead HH (2006) Zinc requirements and the risks and benefits of zinc supplementation. *J Trace Elem Med Biol* 20:3–18.
13. Meunier N, et al. (2005) Importance of zinc in the elderly: The ZENITH study. *Eur J Clin Nutr* 59(Suppl 2):S1–S4.
14. Berg JM, Shi Y (1996) The galvanization of biology: A growing appreciation for the roles of zinc. *Science* 271:1081–1085.
15. Kolenko V, Teper E, Kutikov A, Uzzo R (2013) Zinc and zinc transporters in prostate carcinogenesis. *Nat Rev Urol* 10:219–226.
16. Abnet CC, et al. (2005) Zinc concentration in esophageal biopsy specimens measured by x-ray fluorescence and esophageal cancer risk. *J Natl Cancer Inst* 97:301–306.
17. Prasad AS, et al. (2010) Dietary zinc and prostate cancer in the TRAMP mouse model. *J Med Food* 13:70–76.
18. Banudevi S, et al. (2011) Protective effect of zinc on N-methyl-N-nitrosourea and testosterone-induced prostatic intraepithelial neoplasia in the dorsolateral prostate of Sprague Dawley rats. *Exp Biol Med (Maywood)* 236:1012–1021.
19. Leitzmann MF, et al. (2003) Zinc supplement use and risk of prostate cancer. *J Natl Cancer Inst* 95:1004–1007.
20. Kristal AR, Stanford JL, Cohen JH, Wicklund K, Patterson RE (1999) Vitamin and mineral supplement use is associated with reduced risk of prostate cancer. *Cancer Epidemiol Biomarkers Prev* 8:887–892.
21. Gonzalez A, Peters U, Lampe JW, White E (2009) Zinc intake from supplements and diet and prostate cancer. *Nutr Cancer* 61:206–215.
22. Epstein MM, et al. (2011) Dietary zinc and prostate cancer survival in a Swedish cohort. *Am J Clin Nutr* 93:586–593.
23. Mahmoud AM, et al. (2016) Zinc intake and risk of prostate cancer: Case-control study and meta-analysis. *PLoS One* 11:e0165956.
24. Alder H, et al. (2012) Dysregulation of miR-31 and miR-21 induced by zinc deficiency promotes esophageal cancer. *Carcinogenesis* 33:1736–1744.
25. Croce CM (2009) Causes and consequences of microRNA dysregulation in cancer. *Nat Rev Genet* 10:704–714.
26. Volinia S, et al. (2006) A microRNA expression signature of human solid tumors defines cancer gene targets. *Proc Natl Acad Sci USA* 103:2257–2261.
27. Schaefer A, et al. (2010) Diagnostic and prognostic implications of microRNA profiling in prostate carcinoma. *Int J Cancer* 126:1166–1176.
28. Rottiers V, Näär AM (2012) MicroRNAs in metabolism and metabolic disorders. *Nat Rev Mol Cell Biol* 13:239–250.
29. Eidelman E, Twum-Ampofo J, Ansari J, Siddiqui MM (2017) The metabolic phenotype of prostate cancer. *Front Oncol* 7:131.
30. Dakubo GD, Parr RL, Costello LC, Franklin RB, Thayer RE (2006) Altered metabolism and mitochondrial genome in prostate cancer. *J Clin Pathol* 59:10–16.
31. Hahn P, et al. (1997) The classification of benign and malignant human prostate tissue by multivariate analysis of 1H magnetic resonance spectra. *Cancer Res* 57:3398–3401.
32. Cheng LL, Wu C, Smith MR, Gonzalez RG (2001) Non-destructive quantitation of spermine in human prostate tissue samples using HRMAS 1H NMR spectroscopy at 9.4 T. *FEBS Lett* 494:112–116.
33. Costello LC, Franklin RB (1998) Novel role of zinc in the regulation of prostate citrate metabolism and its implications in prostate cancer. *Prostate* 35:285–296.
34. McCormick DL, et al. (1998) Influence of N-methyl-N-nitrosourea, testosterone, and N-(4-hydroxyphenyl)-all-trans-retinamide on prostate cancer induction in Wistar-Unilever rats. *Cancer Res* 58:3282–3288.
35. Fong LY, et al. (2016) MicroRNA dysregulation and esophageal cancer development depend on the extent of zinc dietary deficiency. *Oncotarget* 7:10723–10738.
36. Taccioli C, et al. (2015) Repression of esophageal neoplasia and inflammatory signaling by anti-miR-31 delivery in vivo. *J Natl Cancer Inst* 107:djv220.
37. Sensibar JA (1995) Analysis of cell death and cell proliferation in embryonic stages, normal adult, and aging prostates in human and animals. *Microsc Res Tech* 30: 342–350.
38. De Marzo AM, et al. (2007) Inflammation in prostate carcinogenesis. *Nat Rev Cancer* 7:256–269.
39. Barnes PJ, Karin M (1997) Nuclear factor-kappaB: A pivotal transcription factor in chronic inflammatory diseases. *N Engl J Med* 336:1066–1071.
40. Hermani A, et al. (2005) Calcium-binding proteins S100A8 and S100A9 as novel diagnostic markers in human prostate cancer. *Clin Cancer Res* 11:5146–5152.
41. Begley LA, et al. (2008) CXCL5 promotes prostate cancer progression. *Neoplasia* 10: 244–254.
42. Gupta S, Srivastava M, Ahmad N, Bostwick DG, Mukhtar H (2000) Over-expression of cyclooxygenase-2 in human prostate adenocarcinoma. *Prostate* 42:73–78.
43. Geiss GK, et al. (2008) Direct multiplexed measurement of gene expression with color-coded probe pairs. *Nat Biotechnol* 26:317–325.
44. Schetter AJ, Heegaard NH, Harris CC (2010) Inflammation and cancer: Interweaving microRNA, free radical, cytokine and p53 pathways. *Carcinogenesis* 31:37–49.
45. Lichten LA, Cousins RJ (2009) Mammalian zinc transporters: Nutritional and physiologic regulation. *Annu Rev Nutr* 29:153–176.
46. Xu XM, et al. (2016) Decreased expression of SLC 39A14 is associated with tumor aggressiveness and biochemical recurrence of human prostate cancer. *OncoTargets Ther* 9:4197–4205.
47. Singh CK, et al. (2016) Analysis of zinc-exporters expression in prostate cancer. *Sci Rep* 6:36772.
48. Hanahan D, Weinberg RA (2011) Hallmarks of cancer: The next generation. *Cell* 144: 646–674.
49. Cancer Genome Atlas Research Network (2015) The molecular taxonomy of primary prostate cancer. *Cell* 163:1011–1025.

50. Denkert C, et al. (2006) Mass spectrometry-based metabolic profiling reveals different metabolite patterns in invasive ovarian carcinomas and ovarian borderline tumors. *Cancer Res* 66:10795–10804.
51. Wikoff WR, et al. (2015) Metabolomic markers of altered nucleotide metabolism in early stage adenocarcinoma. *Cancer Prev Res (Phila)* 8:410–418.
52. Barupal DK, et al. (2012) MetaMapp: Mapping and visualizing metabolomic data by integrating information from biochemical pathways and chemical and mass spectral similarity. *BMC Bioinformatics* 13:99.
53. Kotera M, Hirakawa M, Tokimatsu T, Goto S, Kanehisa M (2012) The KEGG databases and tools facilitating omics analysis: Latest developments involving human diseases and pharmaceuticals. *Next Generation Microarray Bioinformatics. Methods in Molecular Biology (Methods and Protocols)*, eds Wang J, Tan A, Tian T (Humana Press, New York), Vol 802, pp 19–39.
54. Bolton EE, Wang Y, Thiessen PA, Bryant SH (2008) PubChem: Integrated platform of small molecules and biological activities. *Annu Rep Comput Chem* 4:217–241.
55. Sreekumar A, et al. (2009) Metabolomic profiles delineate potential role for sarcosine in prostate cancer progression. *Nature* 457:910–914.
56. Reaves ML, Young BD, Hosios AM, Xu YF, Rabinowitz JD (2013) Pyrimidine homeostasis is accomplished by directed overflow metabolism. *Nature* 500:237–241.
57. Barupal DK, Fiehn O (2017) Chemical similarity enrichment analysis (ChemRICH) as alternative to biochemical pathway mapping for metabolomic datasets. *Sci Rep* 7: 14567.
58. Costello LC, Franklin RB, Feng P, Tan M, Bagasra O (2005) Zinc and prostate cancer: A critical scientific, medical, and public interest issue (United States). *Cancer Causes Control* 16:901–915.